THE JOURNAL OF PHYSICAL CHEMISTRY C

Article

pubs.acs.org/JPCC

Highly Shocked Polymer Bonded Explosives at a Nonplanar Interface: Hot-Spot Formation Leading to Detonation

Qi An, William A. Goddard III,* Sergey V. Zybin, Andres Jaramillo-Botero, and Tingting Zhou

Materials and Process Simulation Center, California Institute of Technology, Pasadena, California 91125, United States

Supporting Information

ABSTRACT: We report reactive molecular dynamics simulations using the ReaxFF reactive force field to examine shock-induced hot-spot formation followed by detonation initiation in realistic (2.7 million atoms) models of polymer bonded explosives (PBX) with nonplanar interfaces. We considered here two energetic materials (EMs) pentaerythritol tetranitrate (PETN), a common EM for PBX, and silicon pentaerythritol tetranitrate (Si-PETN), which is so extremely sensitive that it has not been possible to characterize its shock properties experimentally. In each case the EM was embedded in a hydroxyl-terminated polybutadiene (HTPB) based polymer binder matrix to form a model of PBX that has a periodic sawtooth nonplanar interface. For the cases in which the shock wave propagates from the EM to polymer (EM→poly), we observed that a hot spot arises from shear localization at the convex polymer asperity. For the case in which the shock direction is inverted (shock wave propagates from the polymer to the EM, EM←poly), we find that a hot spot is initiated at the concave polymer asperity and a second more significant hot spot forms at the convex polymer asperity. This second hot spot is enhanced due to converging shock wave interactions with the nonplanar interface. Under the same shock conditions, the first step in the Si-PETN decomposition is the Si−C−O−X rearrangement to Si−O−C−X through a five centered transition state on the Si that releases 45 kcal/mol of energy that leads to a continuous increase of temperature and pressure in the hot-spot region, until detonation. By contrast, the first step for PETN is NO_2 release, which is endothermic by 39 kcal/mol, with the consequence that the hot spot is attenuated by the polymer binder, reaching a steady temperature state involving NO_2 dissociation and HONO formation.

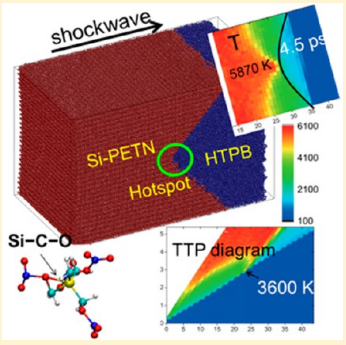

I. INTRODUCTION

The interactions of mechanical shocks with materials lead to a wide range of interesting phenomena such as plastic flow via dislocations or melting for metals, amorphization for ice and silica, instabilities for material with large-density ratio interfaces, and increased chemical activity for energetic materials (EMs).[1−5] In particular, EMs exhibit a broad range of applications in rocket propulsion, civil engineering, and military weapons, in which shock-induced chemistry plays an essential role. It is generally accepted that hot spots form after a shock passes through heterogeneous structures in these materials (e.g., defects, voids, grain boundary, and interfaces)[6−9] increasing the probability of detonation. However, despite extensive experimental and theoretical efforts,[10−17] the mechanism underlying hot-spot formation and their relation to detonation remain controversial because of the complex coupling of thermal, mechanical, and chemical degrees of freedom.

To prevent accidental detonation, explosive powders are normally bound to polymer matrices commonly referred to polymer bonded explosives (PBXs). In a previous study,[16] we examined PBX models of cyclotrimethylene trinitramine (RDX) and hydroxyl-terminated polybutadiene (HTPB) polymer binder with a nonplanar (sawtooth) interface. We found that a hot spot forms via shear localization as the shock wave propagates from the high-density EM to the low-density polymer at the convex polymer asperity of the interface. Similarly, we reported the origin of shock-induced hot spot formation from EM stacking faults.[18]

Here, we report on the shock-induced behavior of a new PBX based on the silapentaerythritol tetranitrate (Si-PETN), which experimentally shows dramatically increased sensitivity, exploding with just a touch of a spatula (no impact), making Si-PETN a useful prototype for atomistic studies of fast energy release and detonation initiation. For comparison, we also report the reactive dynamics for the PBX based on pentaerythritol tetranitrate (PETN) under the same shock conditions.

Si-PETN is structurally identical to PETN, except that the central carbon atom is substituted by silicon. We previously identified[19] from density functional theory (DFT) studies a novel structural rearrangement for the decomposition of Si-PETN that explains the very dramatic increase in sensitivity observed experimentally. We found that Si-PETN leads to a favorable pentacoordinate transition-state in which the Si−C bond breaks to form new Si−O and C−O bonds simultaneously, leading to a transition-state barrier of 33 kcal/mol (for PETN the same reaction has an 80 kcal/mol barrier) that is much lower than the ∼40 kcal/mol barrier for PETN that leads to the O−NO_2 bond fission that is normally observed in such

Received: May 14, 2013
Revised: December 2, 2013
Published: December 2, 2013

dx.doi.org/10.1021/jp404753v | J. Phys. Chem. C 2013, 117, 26551−26561

EMs as RDX and HMX.[20−22] This pentacoordinate Si−O driven mechanism was also demonstrated to be very exothermic (45 kcal/mol) for Si-PETN,[19] leading to a large net energy release at the very first step of decomposition that in turn facilitates a rapid temperature increase and expansion of the reaction zone to lead to early detonation.

In this paper, we consider two PBX models: Si-PETN and PETN, with a nonplanar sawtooth interface between the EM and HTPB polymer binder and use the ReaxFF reactive force field[20] in reactive molecular dynamics (RMD) simulations to examine and compare the hot-spot formation mechanisms as shock waves propagate through the interface. Our simulations elucidate the underlying mechanisms to reveal the dramatic difference in the physical and chemical phenomena for Si-PETN and PETN under the same shock conditions. In particular, we investigated (1) hot-spot formation and evolution arising due to a nonplanar (sawtooth) interface, (2) shock-induced chemical reactions in the hot-spot region, and (3) detonation initiation.

Our results indicate that hot-spot formation leads to detonation initiation, but that detonation progression is highly dependent on the energy release resulting from chemical reactions.

II. RMD SIMULATION DETAILS

II-1. Reactive Force Field Details. ReaxFF uses a bond-order−bond-distance relationship with geometry-dependent charges to describe smoothly chemical reactions processes. The parameters for ReaxFF are determined solely from a large number of quantum mechanical (QM) calculations at the B3LYP level of density functional theory on a diverse set of material bulk phases, surface interactions, reaction barriers, and transition states, among others.[23] The advantage of basing all parameters in ReaxFF on QM is that any surprising results can be tested by simplifying the system to one that can be treated with QM and comparing. If we find ReaxFF to be in error, we merely add the new QM results to the training set and reoptimize until the phenomena is correctly captured. Thus recent improvements over the original ReaxFF formulation have included (1) a general way to handle the Pauli repulsion effects at the inner wall for the very short distances that can occur at very strong impacts (20 km/s) that was not described well by the standard Morse−van der Waals functional form (for which the parameters are more suited to handling the steric interactions for strained bond angles and torsions)[24] and (2) introducing the low-gradient dispersion correction[26,25] that provides a better description of the long-range $1/R^6$ form of the dispersion interactions while avoiding changing the description for the valence interaction regions.

These improved the descriptions had been well-validated for describing the mechanical properties and chemical reactions in various explosives and polymers.[27−31]

This ReaxFF force field for energetic materials incorporates the ReaxFF parameters previously developed for the C−H−O system,[29] which were used successfully to examine C−H−O polymer systems under shock conditions.[27] Specifics on the QM data and reaction pathways captured by this ReaxFF for energetic materials are found in our previous study.[32] (All ReaxFF parameters are collected together in the Supporting Information (SI)). Our MD simulations used the ReaxFF engine incorporated into the large-scale atomic/molecular massively parallel simulator (LAMMPS).[33]

II-2. PBX Model Preparation. The PBX model is similar to the one used by our previous studies[16] where the PETN and Si-PETN crystals were placed in the binder matrix with a sawtooth interface.

The binder consists of hydrogen-terminated polybutadiene (HTPB) and isophorone diisocyanate (IPDI) based polyurethane rubber with dioctyl adipate (DOA) molecules as plasticizer. Each polymer chain has a molecular weight of 1518 Da. We used the cohesive energy density (CED) Monte Carlo method[34] to determine the bulk conformational structure of the polymer at ambient conditions. The DREIDING[35] nonreactive force field was used in the CED process to avoid bond breaking and formation, while charge equilibration was used for the charges.[36] This led to a polymer binder with density of 0.94 g/cm^3 (lattice parameters: a = 21.674 Å, b = 22.337 Å, c = 21.9210 Å, α = 90.536, β = 89.840, and γ = 90.581).

Then we optimized separately the periodic cells of PETN, Si−PETN, and polymer binder using ReaxFF. These structures were equilibrated at room temperature and 1 atm using an NPT ensemble (constant pressure, constant temperature, and constant number of particles). This resulted in lattice constants of a = 9.31 Å, c = 6.73 Å for PETN and a = 9.73 Å, c = 6.96 Å for Si-PETN, which agree well with experimental and ab initio calculation results.[37,38] The resulting densities (Si-PETN, 1.68 g/cm^3; PETN, 1.78 g/cm^3; and HTPB binder, 0.96 g/cm^3) compare well with experimental and ab initio values of 1.75 g/cm^3 at zero K, 1.77 g/cm^3, and 0.96 g/cm^3 at 300 K respectively.

Then we constructed the PBX composite with a sawtooth interface between the Si-PETN and the polymer (HTPB) as follows. Taking the shock direction as x (nonperiodic), we started with Si-PETN supercell with periodic dimensions of 27.2 nm in the y direction and 25.1 nm in the z direction. Then we formed a sawtooth interface for Si-PETN by cutting along the (110) and (1−10) surfaces based on the molecular center of mass.

A complementary surface was built into the HTPB as follows. First the periodic dimensions of the polymer were deformed to

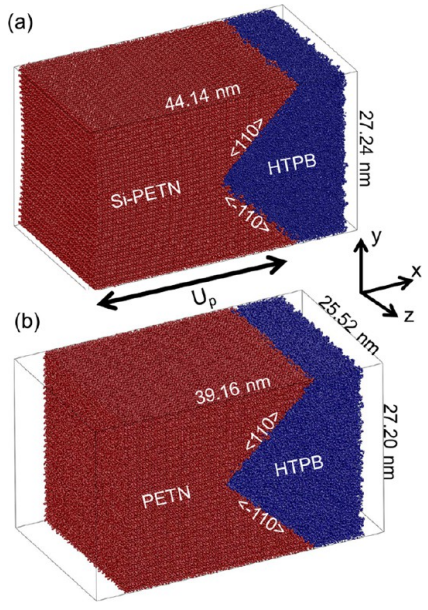

Figure 1. Initial PBX configurations with a sawtooth interface of (a) Si-PETN and (b) PETN. EMs were cut along ⟨110⟩ and ←110> directions and filled with HTPB based polymer binder. Shock propagates along either the x direction (EM to polymer) or the $-x$ direction (polymer to EM).

dx.doi.org/10.1021/jp404753v | J. Phys. Chem. C 2013, 117, 26551−26561

match the 27.2 × 25.1 nm cross-section of the (100) surface. Then each polymer chain having its center of mass within the intended region was kept whole while the others were fully eliminated. This led to some chains extending outside the intended region for the polymer. Then we brought the EM and polymer pieces together to a point expected to have 2% compression of polymer, and we relaxed just the polymer part to form a smooth surface. Finally, we extended the PBX model to have a total thickness in the x direction of 44.1 nm, leading to a total of 2,755,226 atoms.

This Si-PETN−poly system was equilibrated at room temperature using an NVT ensemble (constant volume, constant temperature, and constant number of particles) for 15 ps to eliminate bad contacts at the interface.

The PETN−poly PBX model was constructed using the same procedure. Figure 1 depicts the sawtooth interface models of PBX. The PETN system contains a total of 2,612,122 atoms with cell dimensions of 39.2 nm × 27.2 nm × 25.5 nm, where the EM portion has 1,565,942 atoms and the binder 1,046,180 atoms.

II-3. Details of the Shock Simulation and Analyses. We consider two cases in which shock waves were generated by driving the thermalized two-dimensionally (2D) periodic slabs at velocities of 2.5 or 3.5 km/s onto a reflective wall. The initial shock conditions were obtained by adding the desired particle velocity to the thermal velocities of all atoms in the slab. Periodic boundary conditions were not applied along the shock direction (x-axis). We simulated the shock propagation from the EM to the polymer binder, (EM→poly) and in the opposite direction (EM←poly), using a microcanonical (NVE) ensemble. The equations of motions were integrated for all particles using a 0.1 fs time step with the Verlet algorithm.

To analyze the spatial distributions of physical properties (temperature, stress, and others) during shock loading, we partitioned the simulation cell into fine bins along the x direction (1D-binning analysis) or along the x−y plane (2D-binnning analysis), and then obtained average physical properties within each bin.[16] The center-of-mass velocity of a bin was removed when calculating temperature and stress. Stress for each bin was the averaged virial stress plus thermal contributions. The plots of temperature, stress, and chemical bonds, etc., used two-dimensional bins of 1 nm × 1 nm in the x−y plane but averaging all atoms in the z (periodic) direction to illustrate the effects of the sawtooth interface under shock compression. However, to capture the physical properties near the hot spot, we defined one-dimensional bins passing through the two asperities but just 1 nm × 1 nm in cross-section and averaging all atoms in the z direction. The time evolution of physical properties in the hot-spot region is examined only in one small bin (1 nm × 1 nm in the x−y plane).

Usually molecular simulations determine atomic connectivity by comparing the interatomic distances with the van der Waals (vdW) radii. However, this cannot be used for the highly shocked states since the nonbond dimensions may be greatly reduced from normal values. Thus to analyze chemical reactions, we use the ReaxFF bond order analysis (which ranges from 0 to 1) to define the molecular fragments and to determine when bonds are broken or formed. Generally we consider the bond broken when the bond order goes below 0.3. Here we chose different bond order cutoffs so that the normal vibrations of hot molecules would not exhibit oscillations in fragments sizes for the high temperatures and high pressures. The bond order cutoff table is in the Supporting Information.

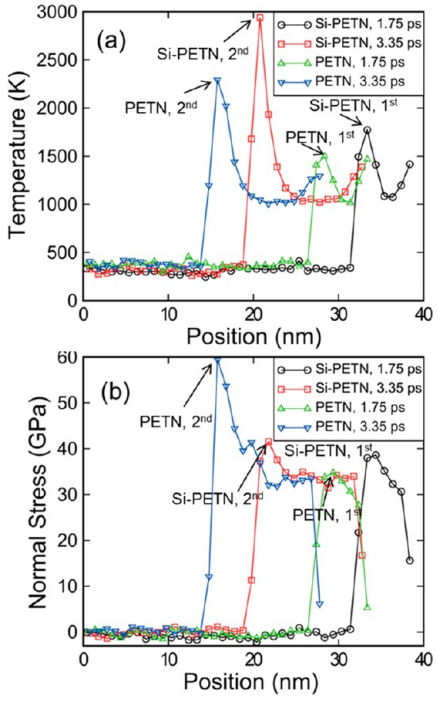

Figure 2. One-dimensional profiles for the cases of shock propagation from low-density polymer to high-density PETN or Si-PETN. The particle velocity is U_p = 3.5 km/s. (a) Temperature: Hotspots form in both asperity regions. The second hot spot has a much higher temperature than the first one. (b) Normal stress: The stress increases in the second hot spot. The positions of hot spots differ by 5 nm between PETN and Si-PETN because the Si-PETN is ∼5 nm thicker than PETN in our PBX models.

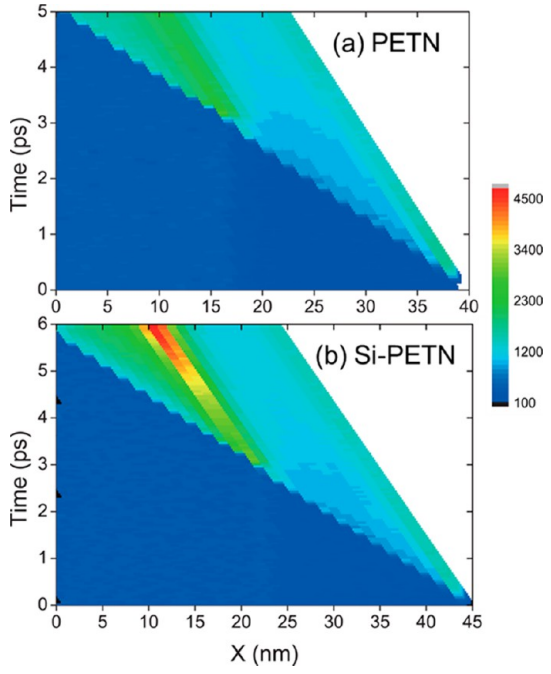

Figure 3. Temperature−time−position diagram for the convex polymer asperity as the shock propagates from low-density polymer to high-density EM with U_p = 3.5 km/s. (a) PETN: The hot spot forms at 3 ps with the temperature remaining stable until 5 ps (and beyond). (b) Si-PETN: The hot spot forms at 3 ps, but its temperature increases rapidly up to 6 ps (and beyond).

dx.doi.org/10.1021/jp404753v | J. Phys. Chem. C 2013, 117, 26551−26561

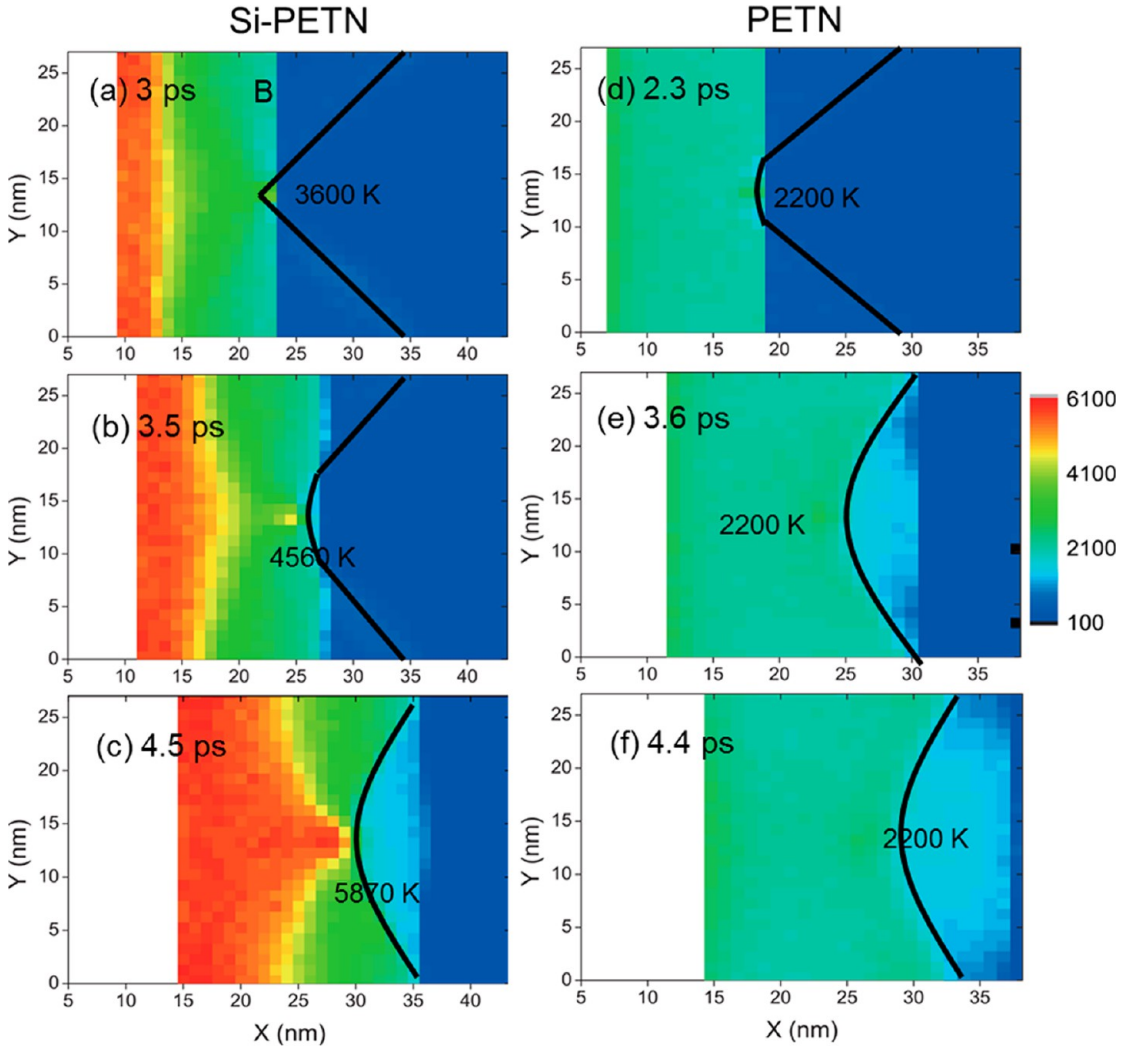

Figure 4. Two-dimensional temperature (K) profiles for Si-PETN (a–c) and PETN (d–f) with U_p = 3.5 km/s as the shock wave propagates from the high-density EM to low-density polymer. The interface of EM and polymer is indicated by the solid line. For Si-PETN, (a) a hot spot forms due to the shear localization at 3.0 ps; (b) the hot-spot temperature increases from 3600 to 4560 K at 3.5 ps, and a second detonation wave forms from the potential wall; and (c) the detonation wave reaches the hot-spot region at 4.5 ps, and the temperature of the hot spot increases to 5870 K. For PETN, (d–f) a hot spot forms with temperature 2200 K at 2.3 ps, but the temperature remains constant with time.

At the transition-state geometry for the pentacoordinate Si–O driven rearrangement in Si-PETN, the silicon atom is bonded to both one oxygen atom and four carbon atoms. Here we define FSiOB (first Si–O bond) as the point at which the silicon atom is bonded to only one oxygen atom along with three or four carbon atoms. To calculate the FSiOB point and the total Si–O bonds distributions, we counted the number of Si–O bonds for the Si atoms and did two-dimensional binning analyses on the x–y plane. Then we normalized the number of Si–O bonds with the total number of Si atoms in each bin to examine the magnitude of chemical reactions.

III. RESULTS AND DISCUSSION

III-1. Shock Propagates from Polymer Binder to Energetic Material (EM←Poly). As the shock propagates from low-density polymer (poly) to high-density energetic material (EM), denoted as (EM←poly), the shock wave first encounters the concave polymer asperity and then the convex polymer asperity.

III-1a. Contact with Initial (Concave) Polymer Asperity. Figure 2a shows the one-dimensional temperature profiles for a small segments (1 nm width) containing the initial (concave) polymer asperity with an impact velocity U_p = 3.5 km/s. We found that a hot spot forms with a temperature increase of 1200 K (leading to 1500 K) for PETN but an increase of 1490 K (leading to 1790 K) for Si-PETN. The mechanism for this hot-spot formation is shear localization as we found before.[16]

For PETN the temperature of this hot spot remains stable at ~1490 K within the first 2.9 ps as displayed in Figure S1 of SI. At 2.9 ps the reflective waves from the wall enhance the hot-spot temperature for PETN from ~1500 to ~1700 K, which we consider to be an artifact

In contrast for Si-PETN the temperature increases from ~1800 to ~2300 K in the first 3 ps. As discussed below in section III-3, this additional temperature increase arises for the extremely exoergic rearrangement of Si–C–O–X to Si–O–C–X, observed in the hot-spot region.

III-1b. Contact with the Second (Convex) Polymer Asperity. For EM←poly shock propagation, we find a new phenomenon as the shock wave continues propagating within the converging width of the sawtooth interface of the low-impedance polymer embedded in the high-impedance

dx.doi.org/10.1021/jp404753v | J. Phys. Chem. C 2013, 117, 26551–26561

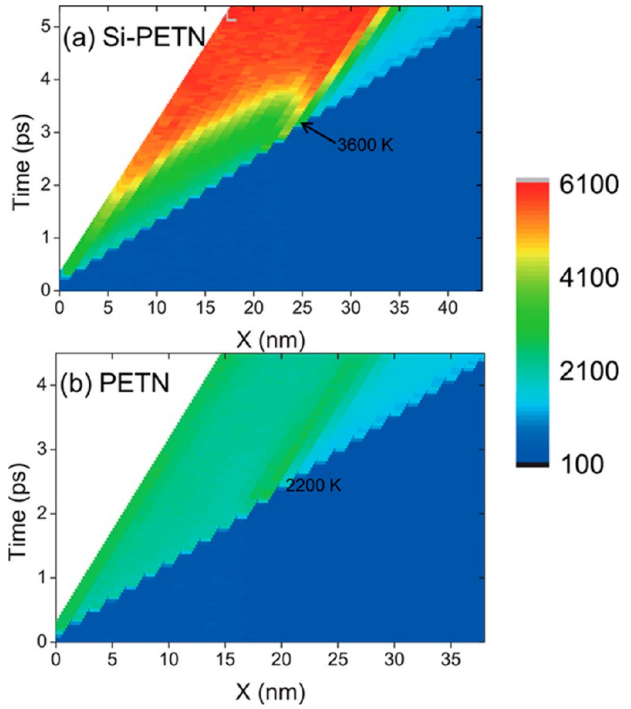

Figure 5. Temperature–position–time diagram for Si-PETN and PETN (convex polymer asperity) as the shock wave propagates from the EM to the polymer binder with U_p = 3.5 km/s. The hot spot forms when the shock encounters the asperity. For PETN the temperature remains constant, but for Si-PETN the temperature increases dramatically due to highly exoergic chemical reactions.

explosive. Here as the shock waves had reaches the second convex polymer asperity a second much hotter hot spot forms with a temperature of 2290 K for PETN and 2940 K for Si-PETN. This is shown in Figure 2a.

Figure 3 displays the temperature–position–time diagram of this second convex polymer asperity for both PETN and Si-PETN. Again, for PETN the hot spot forms and remains at a stable temperature for some finite amount of time (4 ps), while for Si-PETN the hot-spot temperature increases dramatically after formation (due to the same Si–C–O–X to Si–O–C–X rearrangement) with the hot-spot region expanding after 5 ps.

The origin of this second hot spot is understood as follows. As the planar shock enters this sawtooth interface from the low-density polymer to the high-density explosive, the impedance mismatch from low to high across the boundary of the confined region produces reflected waves leading to Mach discs where both pressure and temperature are elevated.[39,40] Figure 2b shows the one-dimensional normal stress profile for both PETN and Si-PETN. The increased normal stress in the second convex polymer asperity region confirms these converging shock effects. The normal stress for PETN increases more than Si-PETN because the PETN has larger density than Si-PETN.

III-2. Shock Propagates from Energetic Material to Polymer Binder (EM→Poly). When the shock propagates from high-density energetic material (EM) to the low-density polymer binder (poly), denoted as (EM→poly), the shock wave first encounters the convex polymer asperity region and later the concave polymer asperity.

III-2a. Contact with Initial (Convex) Polymer Asperity. Figure 4 shows the two-dimensional temperature profiles for Si-PETN (panels a–c) and PETN (panels d–f) for the EM→poly with U_p = 3.5 km/s. For Si-PETN, we found a hot spot with temperature 3600 K (an increase of 3300K) as the shock wave passes through this convex polymer asperity at 3.0 ps. This hot-spot temperature increases to 4560 K at 3.5 ps and to 5870 K at 4.5 ps indicating the enhancement of the hot spot from chemical reactions induced by the shock.

On the other hand, for the PETN, a cooler hot spot forms with 2200 K at 2.3 ps, this temperature remains stable for times up to 5 ps as the shock passes through the simulation cell, consistent with our previous results.[16]

The hot-spot temperature evolutions (temperature–position–time diagram) for Si-PETN and PETN are shown in Figure 5a,b. For Si-PETN a much hotter hot spot forms whose temperature increase rapidly, while for PETN the hot-spot temperature remains stable. This much hotter hot spot combined with the rapidly increasing temperature observed for Si-PETN explains why Si-PETN is far more sensitive than PETN, as observed experimentally.

Figure 6 shows the normal stress (σ_{11}) profile for Si-PETN (a–c) and PETN (d,e) with U_p = 3.5 km/s. For Si-PETN, the normal stress relaxes from 37.9 GPa (at 2.8 ps) to 35.1 GPa (at 3.0 ps) through the rarefaction wave from the polymer binder, but it increases to 43.1 GPa at 3.5 ps due to kinetics (temperature) effects as the hot-spot temperature increases.

For PETN, the polymer binder also relaxes the normal stress from 45.8 GPa at 1.9 ps to a value of 32.1 GPa at 2.3 ps after the shock wave passes through. Later, it increases to 41.5 GPa at 3.6 ps because of the artifact caused by the reflective wave from the wall (not a result from hot-spot reactivity).

The shear stress profiles for Si-PETN and PETN in Figure S2 of the SI show that for both cases the shear stress relaxes within the hot-spot region. The hot spot arises from is local shear relaxation, which is consistent with the mechanism reported previously.[16]

III-2b. Contact with the Second (Concave) Polymer Asperity (EM→Poly). As the shock encounters the second (concave) polymer asperity region, no hot spot forms for both Si-PETN and PETN as shown in Figure 4c,e. SI Figure S3 shows the one-dimensional temperature profiles for Si-PETN at 4.5 ps and PETN at 3.6 ps with U_p = 3.5 km/s. The temperatures at the second polymer asperity region for PETN and Si-PETN are ~2000 and ~2200 K, respectively, which are similar to the shocked states of intact crystals. The hot-spot temperature for PETN and Si-PETN are 500 and 410 K higher than found in the same asperity as the shock propagates in the opposite direction (from polymer to explosives, section III-1a). The temperature of the shocked EMs is much lower when shock propagates from polymer to EMs than the direct propagation among EMs. This is because polymer is much softer than EMs and the reflective wave at the interface of EM and polymer dissipates some amount of energy as shock wave passes through.

III-3. Sensitive Hotspot and Detonation Initiation in Si-PETN based PBXs (EM→Poly). *III-3a. U_p = 3.5 km/s.* For Si-PETN, Figure 4b shows that second high-temperature wave forms behind the shock wave that shows nonplanar character. This nonplanar wave originates from rarefaction waves at the nonplanar interface. As the shock encounters the sawtooth interface, a nonplanar rarefaction wave is generated from the impedance mismatch between EM and polymer. The rarefaction wave propagates back toward the EM region, enhancing chemical reactivity by relaxing the highly compressed bonds. The enhanced reactivity accelerates the second wave along the interfacial asperity direction where the rarefaction wave interacts with it, leading to the nonplanar character. This

dx.doi.org/10.1021/jp404753v | J. Phys. Chem. C 2013, 117, 26551–26561

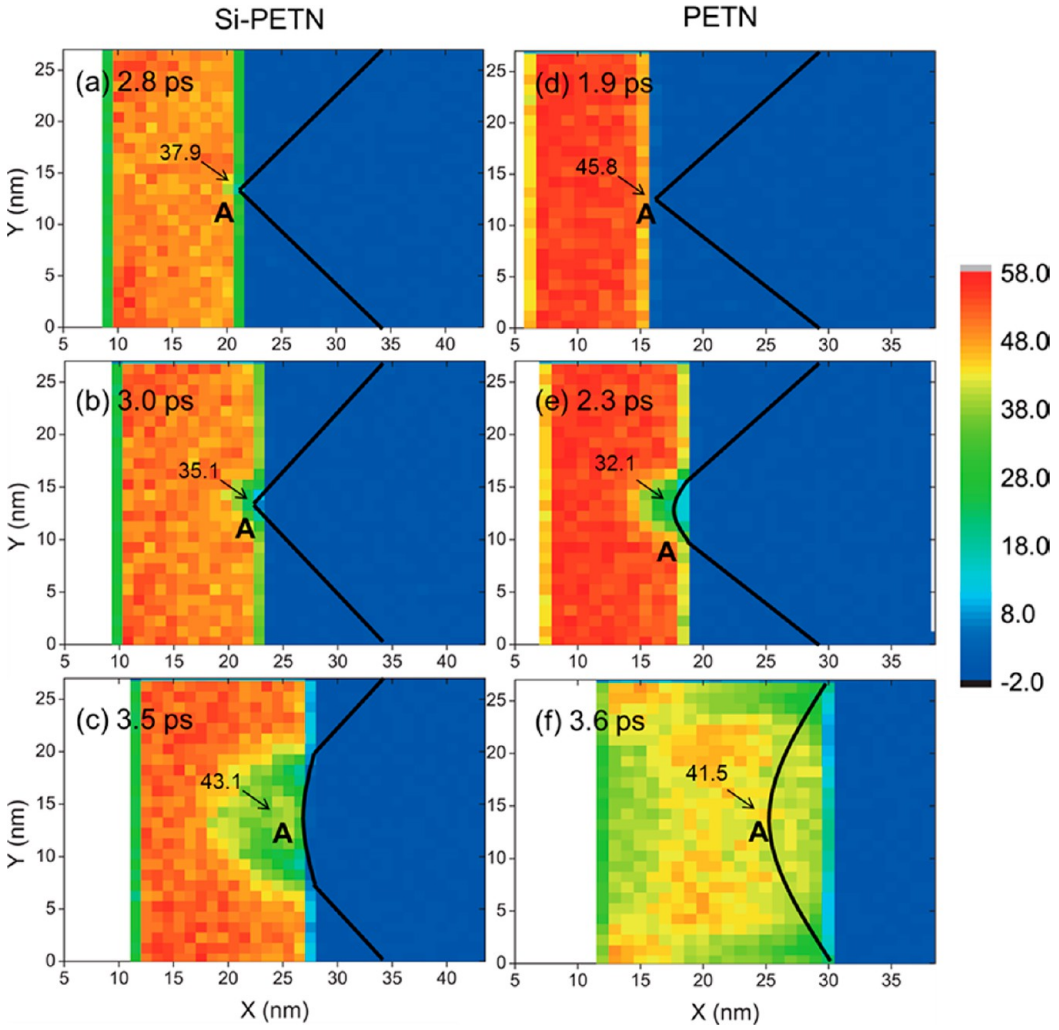

Figure 6. Two-dimensional profiles of the normal stress (GPa) for Si-PETN (a–c) and PETN (d–f) for shock compression from EM to polymer with U_p = 3.5 km/s. The hot-spot region is marked as "A". The polymer–EM interface is represented with the solid line. For Si-PETN (a, b) and PETN (d, e), the normal stress in the hot-spot region is relaxed by the polymer binder as the shock passes through the asperity. (c) For Si-PETN the pressure increases dramatically due to the rapid energy release, whereas for PETN the pressure increase is modest.

rarefaction wavefront can be identified from the normal stress profile in Figure 6b. It is at exactly the same position of the nonplanar detonation wavefront. This phenomenon is not observed in PETN because the high-temperature wave in Si-PETN originates from the extremely exoergic chemical reactions that are absent in PETN (within this early time scale). It is interesting to note that the temperature increase of the non-hot-spot region from the shock compression for Si-PETN is similar to PETN (marked as B in Figure 4a), but it is increased quickly by the second wave.

Figure 7a shows the temperature evolution of hot-spot region. For Si-PETN with U_p = 3.5 km/s, the temperature increases dramatically from 300 to 4120 K in region AB due to the shock compression, followed by a temperature decrease in region BC from 4120 to 3950 K via polymer relaxation, and finally in region CD undergoes a dramatic temperature increase. For PETN, the temperature shows a similar character as the shock passes through, but the temperature reaches a constant value region (2100 K) after polymer relaxation.

Figure 7b shows the evolution of the normal stress which is similar to the temperature evolution. The shock stress for PETN is initially higher than for Si-PETN because PETN has a higher initial density. But the normal stress of Si-PETN quickly increases to become larger than PETN in region CD. Since the Si-PETN crystal is ∼5 nm longer than the PETN in the two PBX models, the hot-spot formation time for Si-PETN is ∼3.1 ps compared to ∼1.8 ps for PETN

III-3b. U_p = 2.5 km/s. Considering now a piston velocity 2.5 km/s rather than 3.5 km/s, we find that Si-PETN leads to similar behavior, but less extreme: the hot-spot temperature is ∼1900 K as the shock propagates in region AB and the temperature increases in region CD are only 400 K (compared with ∼2000 K for U_p = 3.5 km/s). For PETN the temperature and stress also show the same behavior as for 3.5 km/s, but less extremes.

III-3c. Energetics. We consider now the changes in enthalpy, which is the sum of internal energy and PV. This is related to the energy release in the hot-spot formation and detonation.

Figure 7c shows the enthalpy evolution of the part hot-spot region which is contact with the polymer binder for both Si-PETN and PETN

Figure 8 shows the enthalpy–position–time diagram of the segment including the whole hot-spot region for Si-PETN and for PETN.

Si-PETN Analysis. For Si-PETN, Figure 7c shows that the enthalpy of the region close to polymer dramatically increases for

dx.doi.org/10.1021/jp404753v | J. Phys. Chem. C 2013, 117, 26551–26561

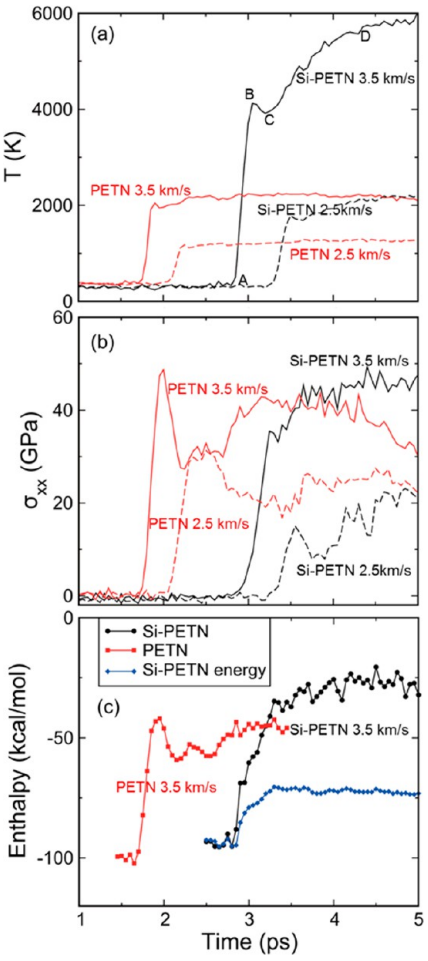

Figure 7. Evolution of physical properties (T, P, H) in the hot-spot region for Si-PETN and PETN for shock compression from EM to polymer. (a) Temperature: For Si-PETN with U_p = 3.5 km/s, AB is the shock compression regime, BC is the polymer relaxation regime, and CD is the regime of fast energy release. This character is much less pronounced with low particle velocity of 2.5 km/s. PETN shows a similar character in the AB and BC regimes but shows a constant temperature for the CD regime. (b) Normal stress and (c) enthalpy show similar character with temperature for Si-PETN and PETN. The blue line is the enthalpy contribution from internal energy.

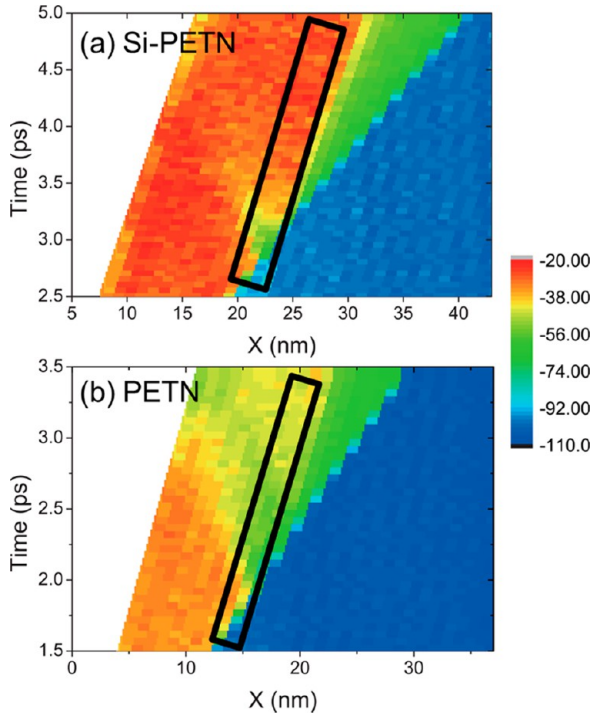

Figure 8. Enthalpy−position−time diagram for Si-PETN and PETN for shock compression from EM to polymer with U_p = 3.5 km/s. The hot-spot region is within the rectangle. (a) For Si-PETN, the enthalpy increases continuously because of the dramatically exoergic chemical reactions. (b) For PETN, the enthalpy is relaxed by the polymer so that it remains relatively constant, as consistent with the temperature evolution.

Si-PETN by 60 kcal/mol between 2.85 and ∼3.25 ps (including shock compression and polymer relaxation) due to the increase of pressure and internal energy, followed a continuous increase region. This continuous enthalpy increase arises mainly from the pressure increase due to the highly energetic chemical reactions. The internal energy decreases slightly during this regime.

Figure 8a displays the enthalpy of the hot-spot region that is far from polymer, showing a dramatic increase as the shock wave passes through the convex polymer asperity region (∼2.8 ps), then the enthalpy decreases near the polymer due to relaxation (∼3.0 ps), and finally it increases thereafter due to the chemical reactions (∼3.2 ps).

Figure 7c shows just part of hot-spot region that is in contacted with the polymer. Here the enthalpy continuously increases with time. This is consistent with the right part in the insert of Figure 8a.

PETN analysis. For PETN, Figure 7c and Figure 8b both indicate that the enthalpy also increases significantly when the shock wave encounters the convex polymer asperity (∼1.8 ps).

Then the polymer binder relaxation maintains a constant enthalpy until 2.7 ps.

At 2.7 ps, the reflective wave from the wall interacts with the hot spot, leading to a 20% increase. We disregard this enthalpy increase for PETN after 2.7 ps because the reflective wave, generated as the rarefaction wave encounters the reflective wall, increases the pressure of the hot-spot region. This leads to an artificial enthalpy increase for PETN as it reaches steady state.

III-3d. Chemistry. To determine the chemistry (and energy release) involved during the hot-spot formation and detonation processes, we analyzed the chemical reactions as the shock waves pass through. Here we selected as the prototype two EM molecules in the hot-spot region for U_p = 3.5 km/s (Figure 9).

For Si-PETN, the pentacoordinate Si−O driven rearrangement of releases ∼45 kcal/mol.[18] This huge energy release subsequently leads to formation of NO_2 and CH_2O, leaving behind a $SiC_3H_6N_3O_9$ fragment that subsequently reacts and breaks down completely.

For PETN, the initial reaction leads only to NO_2 dissociation while releasing just ∼13 kcal/mol of energy, leaving behind two PETN radical fragments, but without changing the overall molecular geometry.

Thus the very exoergic reactions and complete decomposition for Si-PETN leads to detonation, while for PETN the much less exoergic unimolecular NO_2 dissociation reaction leads to a hot spot whose temperature is stable for several picoseconds.

To examine the evolution of the chemistry underlying detonation initiation, we calculated the rate of Si−O bond as-formation during shock propagation. Figure 10 shows the two-dimensional Si−O bond spatial distribution, which we find correlates very well with the temperature distribution in Figure 4.

(a) Initially, many Si−O bonds form in the shocked region before the shock encounters the convex polymer asperity region.

dx.doi.org/10.1021/jp404753v | J. Phys. Chem. C 2013, 117, 26551−26561

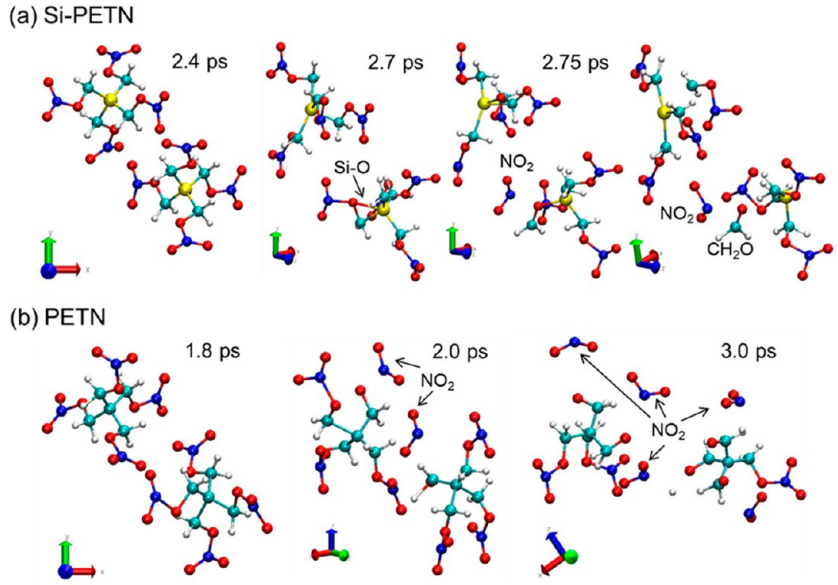

Figure 9. Snapshots from the reactive dynamics trajectory showing prototypical initial chemical reactions of Si-PETN and PETN as the shocks pass through the hot-spot region (shock compression from EM to polymer). Here Si, C, H, O, and N are represented by the yellow, cyan, white, red, and blue filled balls. The shock propagates along the $+x$ direction with U_p = 3.5 km/s. (a) For Si-PETN, the pentacoordinate Si−C−O−X to Si−O−C−X rearrangement leads to NO_2 dissociation and CH_2O formation. (b) For PETN, the collision with a second PETN molecule leads to NO_2 dissociation but no additional fragmentation.

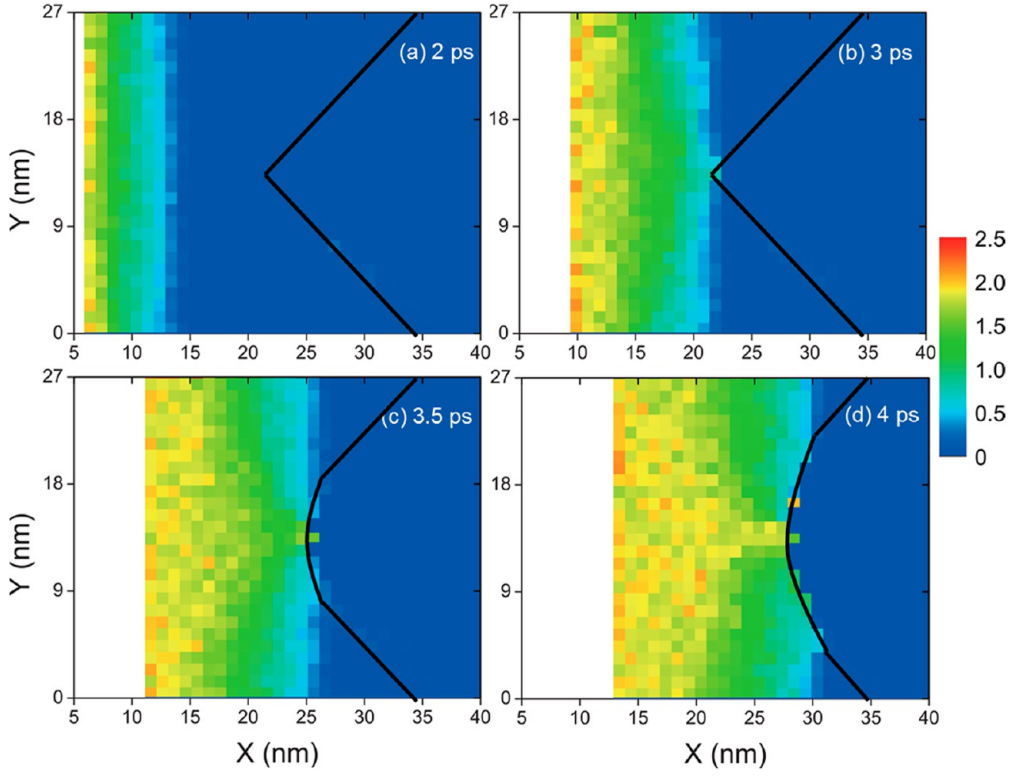

Figure 10. Si-PETN: the spatial distribution of Si−O bonds at various times as shock compression proceeds from EM to polymer with U_p = 3.5 km/s. The interface of EM and polymer is represented by the solid line. The number of Si−O bonds is normalized by the total number of Si atoms in each bin. (a) This is the distribution before hot-spot formation; (b) the shock wave encounters the convex polymer asperity and a hot spot forms; (c) a second high-temperature wave enters the hot-spot region; (d) The second wave passes through the hot-spot region.

(b) Then at 3 ps the shock wave encounters the convex polymer asperity leading to increased Si−O bonds and hot-spot formation.

(c) Then, at 3.5 ps the high-temperature wave develops to a nonplanar wave in the Si-PETN region due to the rarefaction wave in the nonplanar interface. Each Si atom tends to form two Si−O bonds in the high-temperature regions.

(d) In addition small numbers of Si−O bonds form at the Si-PETN/polymer interface because of the high interfacial energy and low energy barrier for carbon−oxygen rearrangement.

dx.doi.org/10.1021/jp404753v | J. Phys. Chem. C 2013, 117, 26551−26561

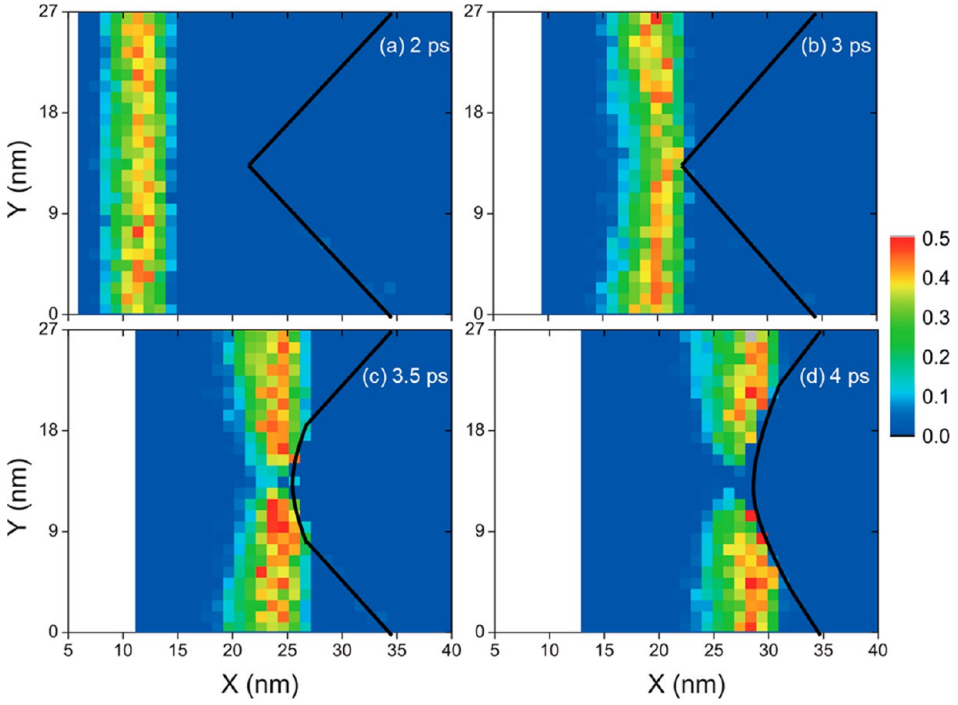

Figure 11. Si-PETN: the distribution of the events at which the first Si−O bond is formed for various times with shock compression from EM to polymer at U_p = 3.5 km/s. The number of Si−O bonds is normalized by the total number of Si atoms in each bin. The interface of EM and polymer is represented by the solid line. (a) This is the distribution before hot-spot formation; (b) the shock wave encounters the convex polymer asperity; (c) the shock has passed through the hot spot; (d) a hot spot develops to initiate detonation. Some Si−O bonds also form at the interface between the EM and polymer.

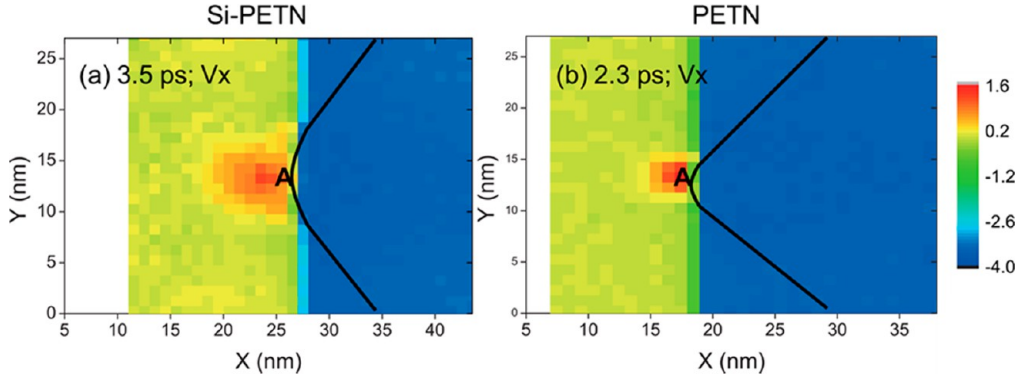

Figure 12. Two-dimensional velocity profiles of Si-PETN (a) and PETN (b) with shock compression from EM to polymer at U_p = 3.5 km/s. The hot-spot region is marked as A. The interface of EM and polymer is represented by the solid line. These profiles indicate that the interfacial perturbations for Si-PETN (a) and PETN (b) are due to the impedance mismatch of EMs and polymer.

The first Si−O bond (FSiOB) formation in Si-PETN molecule plays important roles in the initial chemical reactions. Figure 11 shows the two-dimensional spatial distributions for FSiOB. The shock compression triggers a few uniformly distributed FSiOBs as the shock wave passes through, but the maximum number appears ∼2 nm behind the shock front. No FSiOBs exist behind ∼10 nm of the shock front. Much fewer FSiOBs but a larger total number of Si−O bonds were observed in the hot-spot region. Although first Si−O bond formation is essential, it is not correlated with the temperature profile. These results indicate that FSiOB formation kinetically induces the subsequent chemical reactions, while the steps following additional Si−O bond formations release the majority of the energy that builds the detonation toward initiation and propagation process.

The chemical reactions in Si-PETN lead to interface perturbations that might lead to enhanced Richtmyer−Meshkov interfacial instabilities. Figure 12 shows the two-dimensioanl velocity distribution. The velocity along the x direction displays a similar character for both Si-PETN and PETN: moving the EM into the polymer region causes an interfacial perturbation. The interfacial perturbation (SI Figure S4) is much more significant for Si-PETN because of the much stronger chemical reactions. This likely leads to jetting nucleation.

IV. CONCLUSION

We used reactive molecular dynamics (RMD) to examine the mechanical, chemical, and thermal response of mechanically shocked polymer bonded explosives (PBXs) using a realistic model of a nonplanar (sawtooth) interface with ∼2.7 million

dx.doi.org/10.1021/jp404753v | J. Phys. Chem. C 2013, 117, 26551−26561

independent atoms. We observed the formation of one hot spot at the sawtooth convex polymer asperity when the shock wave propagates from the high-density EM to the low-density binder. But we found hot spots at both polymer asperities when the shock wave propagates in the opposite direction. We observed that for PETN the hot spots reach a steady temperature state by 6 ps, while for Si-PETN within the first few picoseconds an enhanced hot spot is observed whose temperature continues to increase dramatically with time.

The difference in response for PETN and Si-PETN arises from the difference in the chemical reactions induced by shock compression. For Si-PETN, the pentacoordinate Si−O driven mechanism leads to silicon−carbon−oxygen rearrangements that dramatically increase energy release, leading to a hot spot whose temperature increases dramatically with time. In contrast for PETN the initial reaction is NO_2 dissociation from unimolecular decomposition that initially absorbs energy leading to a hot spot whose temperature remains stable within the simulation time scale.

■ ASSOCIATED CONTENT

Supporting Information

Text giving the ReaxFF parameters, table listing bond-order cutoff for bond fragment analyses, and figures of temperature−time−position diagram for the shock met with the first convex polymer asperity from polymer to EMs with U_p = 3.5 km/s, two-dimensional shear stress profile of Si-PETN and PETN for the first concave polymer hot spot when shock propagates from EMs to polymer with U_p = 3.5 km/s, one-dimensional temperature profiles for Si-PETN and PETN when shocks encounter the second (convex) polymer asperity region from explosives to polymer with U_p = 3.5 km/s, and the initiation of interfacial instabilities of Si-PETN. This material is available free of charge via the Internet at http://pubs.acs.org.

■ AUTHOR INFORMATION

Corresponding Author

*E-mail: wag@wag.caltech.edu.

Notes

The authors declare no competing financial interest.

■ ACKNOWLEDGMENTS

All computations were carried out on the Army HPC systems. We thank Betsy Rice and Larry Davis for assistance. Personnel were supported by ARO (Grants W911NF-05-1-0345 and W911NF-08-1-0124) and by ONR (Grant N00014-09-1-0634). In addition A.J.-B. and W.A.G. received support from the PSAAP project at Caltech (Grant DE-FC52-08NA28613). We thank Mr. Wei-Guang Liu at Caltech for the useful discussions.

■ REFERENCES

(1) Ball, P. Material witness: Shock relief. *Nat. Mater.* **2012**, *11*, 747.

(2) Holian, B. L.; Lomdahl, P. S. Plasticity Induced by Shock Waves in Nonequilibrium Molecular-Dynamics Simulations. *Science* **1998**, *280*, 2085−2088.

(3) Germann, T. C.; Holian, B. L.; Lomdahl, P. S.; Ravelo, R. Orientation Dependence in Molecular Dynamics Simulations of Shocked Single Crystals. *Phys. Rev. Lett.* **2000**, *84*, 5351−5354.

(4) Strachan, A.; van Duin, A. C. T.; Chakraborty, D.; Dasgupta, S.; Goddard, W. A., III Shock Waves in High-Energy Materials: The Initial Chemical Events in Nitramine RDX. *Phys. Rev. Lett.* **2003**, *91*, No. 098301.

(5) An, Q.; Luo, S. N.; Han, L. B.; Zhng, L. Q.; Tschauner, O. Melting of Cu under hydrostatic and shock wave loading to high pressures. *J. Phys: Condes. Matter* **2008**, *20*, No. 095220.

(6) Dear, J. P.; Field, J. E.; Walton, A. J. Gas Compression and Jet Formation in Cavities Collapsed by a Shock Wave. *Nature (London)* **1988**, *332*, 505−508.

(7) Chéret, R. *Detonation of Condensed Explosives*; Springer-Verlag: New York, 1993.

(8) Bowden, F. P.; Yoffe, A. D. *Initiation and Growth of Explosions in Liquids and Solids*; Cambridge University Press: Cambridge, England, 1952.

(9) Maffre, P.; Peyrard, M. Molecular-Dynamics Investigations of Shock-Induced Detonations in Inhomogeneous Energetic Crystals. *Phys. Rev. B* **1992**, *45*, 9551−9561.

(10) Field, J. E. Hot Spot Ignition Mechanisms for Explosives. *Acc. Chem. Res.* **1992**, *25*, 489−496.

(11) Field, J. E.; Bourne, N. K.; Palmer, S. J. P.; Walley, S. M.; Sharma, J.; Beard, B. C. Hot-Spot Ignition Mechanisms for Explosives and Propellants. *Philos. Trans. R. Soc. London, Ser. A* **1992**, *339*, 269−283.

(12) Holian, B. L.; Germann, T. C.; Maillet, J. B.; White, C. T. Atomistic Mechanism for Hot Spot Initiation. *Phys. Rev. Lett.* **2002**, *89*, 285501.

(13) Mintmire, J. W.; Robertson, D. H.; White, C. T. Molecular-Dynamics Simulations of Void Collapse in Shocked Model-Molecular Solids. *Phys. Rev. B* **1994**, *49*, 14859−14864.

(14) Nomura, K.; Kalia, R. K.; Nakano, A.; Vashishta, P. Reactive Nanojets: Nanostructure-Enhanced Chemical Reactions in a Defected Energetic Crystal. *Appl. Phys. Lett.* **2007**, *91*, 183109.

(15) Hatano, T. Spatiotemporal Behavior of Void Collapse in Shocked Solids. *Phys. Rev. Lett.* **2004**, *92*, No. 015503.

(16) An, Q.; Zybin, S. V.; Goddard, W. A., III; Jaramillo-Botero, A.; Blanco, M.; Luo, S. N. Elucidation of the Dynamics for Hot-Spot Initiation at Nonuniform Interfaces of Highly Shocked Materials. *Phys. Rev. B* **2011**, *84*, 220101(R).

(17) Tokmakoff, A.; Fayer, M. D.; Dlott, D. D. Chemical Reaction Initiation and Hot-Spot Formation in Shocked Energetic Molecular Materials. *J. Phys. Chem.* **1993**, *97*, 1901−1913.

(18) Jaramillo-Botero, A.: An, Q.; Theofanis, P. L.; Goddard, W. A., III Large-Scale Reactive Molecular Simulation of Hypervelocity Impact of Materials. *Procedia Engineering*, Hypervelocity Impact Symposium 2012, Baltimore, MD, Sep. 17, 2012; Elsevier: Amsterdam, 2012.

(19) Liu, W. G.; Zybin, S. V.; Dasgupta, S.; Klapotke, T. M.; Goddard, W. A., III Explanation of the Colossal Detonation Sensitivity of Silicon Pentaerythritol Tetranitrate (Si-PETN) Explosive. *J. Am. Chem. Soc.* **2009**, *131*, 7490−7491.

(20) Chakraborty, D.; Muller, R. P.; Dasgupta, S.; Goddard, W. A., III The Mechanism for Unimolecular Decomposition of RDX (1,3,5-Trinitro-1,3,5-triazine), an ab Initio Study. *J. Phys. Chem. A* **2000**, *104*, 2261−2272.

(21) Chakraborty, D.; Muller, R. P.; Dasgupta, S.; Goddard, W. A., III Mechanism for Unimolecular Decomposition of HMX (1,3,5,7-Tetranitro-1,3,5,7-tetrazocine), an ab Initio Study. *J. Phys. Chem. A* **2001**, *105*, 1302−1314.

(22) Chakraborty, D.; Muller, R. P.; Dasgupta, S.; Goddard, W. A., III. A Detailed Model for the Decomposition of Nitramines: RDX and HMX. *J Comput.-Aided Mater. Des.* **2001**, *8*, 203−212.

(23) Van Duin, A. C. T.; Dasgupta, S.; Lorant, F.; Goddard, W. A., III. ReaxFF: A Reactive Force Field for Hydrocarbons. *J. Phys. Chem. A* **2001**, *105*, 9396−9409.

(24) Jaramillo-Botero, A.; An, Q.; Cheng, M. J.; Goddard, W. A., III.; Beegle, L. W.; Hodyss, R. Hypervelocity Impact Effect of Molecules from Enceladus' Plume and Titan's Upper Atmosphere on NASA's Cassini Spectrometer from Reactive Dynamics Simulation. *Phys. Rev. Lett.* **2012**, *109*, 213201.

(25) Liu, L. C.; Liu, Y.; Zybin, S. V.; Sun, H.; Goddard, W. A., III ReaxFF-lg: Correction of the ReaxFF Reactive Force Field for London Dispersion, with Applications to the Equations of State for Energetic Materials. *J. Phys. Chem. A* **2011**, *115*, 11016−11022.

(26) Liu, Y.; Goddard, W. A., III. First-Principles-Based Dispersion Augmented Density Functional Theory: From Molecules to Crystals. *J. Phys. Chem. Lett.* **2010**, 2550−2555.
(27) Zybin, S. V.; Goddard, W. A., III.; Xu, P.; van Duin, A. C. T.; Thompson, A. P. Physical Mechanism of Anisotropic Sensitivity in Pentaerythritol Tetranitrate from Compressive-Shear Reaction Dynamics Simulations. *Appl. Phys. Lett.* **2010**, *96*, 081918.
(28) An, Q.; Liu, Y.; Zybin, S. V.; Kim, H.; Goddard, W. A., III Anisotropic Shock Sensitivity of Cyclotrimethylene Trinitramine (RDX) from Compress-and-Shear Reactive Dynamics. *J. Phys. Chem. C* **2012**, *116*, 10198−10206.
(29) Nomura, K. I.; Kalia, R. K.; Nakano, A.; Vashishta, P.; van Duin, A. C. T.; Goddard, W. A., III. Dynamic Transition in the Structure of an Energetic Crystal during Chemical Reactions at Shock Front Prior to Detonation. *Phys. Rev. Lett.* **2007**, *99*, 148303.
(30) Chenoweth, K.; van Duin, A. C. T.; Goddard, W. A., III. ReaxFF reactive force field for molecular dynamics simulations of hydrocarbon oxidation. *J. Phys. Chem. A* **2008**, *112*, 1040−1054.
(31) Mattsson, T. R.; Lane, J. M. D.; Cochrane, K. R.; Desjarlais, M. P.; Thompson, A. P.; Pierce, F.; Grest, G. S. First-principles and classical molecular dynamics simulation of shocked polymers. *Phys. Rev. B* **2010**, *81*, 054103.
(32) Zhou, T. T.; Liu, L. C.; Goddard, W. A., III.; Zybin, S. V.; Huang, F. L. ReaxFF Reaction Dynamics on Silicon Pentaerythritol Tetranitrate (Si-PETN) Crystal Validates the Mechanism for the Colossal Sensitivity. *J. Phys. Chem. A* **2013**, submitted for publication.
(33) Plimpton, S. Fast Parallel Algorithms for Short-Range Molecular Dynamics. *J. Comput. Phys.* **1995**, *117*, 1−19.
(34) Cozmuta, I.; Blanco, M.; Goddard, W. A., III. Gas Sorption and Barrier Properties of Polymeric Membranes from Molecular Dynamics and Monte Carlo Simulations. *J. Phys. Chem. B* **2007**, *111*, 3151−3166.
(35) Mayo, S. L.; Olafson, B. D.; Goddard, W. A., III. DREIDING: A Generic Force Field for Molecular Simulations. *J. Phys. Chem.* **1990**, *94*, 8897−8909.
(36) Rappé, A. K.; Goddard, W. A., III. Charge Equilibration for Molecular Dynamics Simulations. *J. Phys. Chem.* **1991**, *95*, 3358−3363.
(37) Booth, A. D.; Llewellyn, F. J. The Crystal Structure of Pentaerythritol Tetranitrate. *J. Chem. Soc.* **1947**, 837−846.
(38) Lin, Y.; Budzevich, M. M.; Landerville, A. C.; Oleynik, I. I.; White, C. T. Physical and Chemical Properties of a New Energetic Materials SiPETN. *AIP Conf. Proc.* **2009**, *1195*, 474−477.
(39) Setchell, R. E.; Storm, E.; Sturtevant, B. An Investigation of Shock Strengthening in a Conical Convergent Channel. *J. Fluid Mech.* **1972**, *56*, 505−522.
(40) Brown, J. L.; Ravichandran, G. Shock Waves in Converging Geometries. *AIP Conf. Proc.* **2009**, *1195*, 747−750.